CHAPTER 5
SEMI-ACTIVE SYSTEMS AND APPLICATIONS

If you wish to control the future, study the past...
- Confucius

This chapter describes different semi-active strategies developed for optimal functioning of TLCDs. These strategies include *gain-scheduling* and *clipped optimal* schemes with *continuously-varying* and *on-off* control. It is shown that such systems provide a significant improvement over the performance of a passive system. Numerous examples and applications are provided to elucidate the theory.

5.1 Introduction

Semi-active control systems were first reported in civil engineering structures by Hrovat *et al.* (1983). In other fields such as automotive vibration control, considerable research has been done on semi-active systems (Ivers and Miller, 1991; Karnopp, 1990). A number of devices are currently being studied in the area of structural control, namely the variable stiffness devices, controllable fluid dampers, friction control devices, fluid viscous devices, etc. Recent papers in this area provide a state-of-the-art review of semi-active control devices for vibration control of structures (Spencer and Sain, 1997; Symans and Constatinou, 1999; Kareem *et al*. 1999).

Optimization studies discussed in chapter 3 show that there exist optimal damping and tuning ratio, which lead to high performance of TLCDs. One of the main features of these dampers is that the damping is nonlinearly dependent on the amplitude of excitation.

This chapter proposes two strategies which can improve over the performance of passive systems. One of them involves *gain-scheduling* of the damping based on the feedforward information of the disturbance. The other is a *clipped optimal* system with *continuously-varying* and *on-off* control, which involves a continuos changing of the damping based on feedback of the structural response.

5.2 Gain-scheduled Control

This section discusses a semi-active system which is useful for disturbances which are of long duration and slowly varying (e.g., wind excitations) and where steady-state response is the controlling objective. The optimal head loss coefficient as a function of the loading intensity is described as a *look-up* table. As the loading intensity changes, the headloss coefficient of the TLCD is changed in real-time in accordance with this *look-up* table by changing the valve/orifice opening.

Gain-scheduling is defined as a special type of non-linear feedback, with a non-linear regulator whose parameters are changed as a function of the operating conditions in a pre-programmed manner. As shown in Fig. 5.1, the regulator is tuned for each operating condition. Though *gain-scheduling,* an open-loop compensation technique, may be time consuming to design, its regulator parameters can be changed very quickly in response to system changes. This kind of control is more commonly used in aerospace and process control applications (Astrom and Wittenmark, 1989).

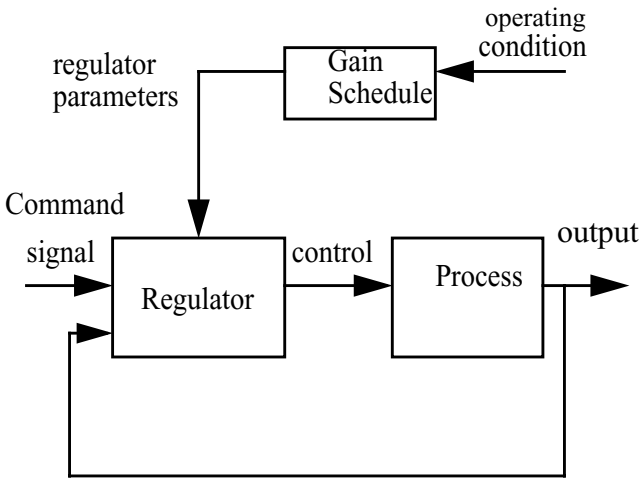

Figure 5.1 Gain scheduling concept

5.2.1 Determination of Optimum Headloss Coefficient

The procedure for estimating the optimum damping coefficient, ζ_{opt}, for TLCDs under a host of loading conditions was outlined in chapter 3. In this section, methods to determine the optimal headloss coefficient (ξ_{opt}) is presented. This is the parameter responsible for introducing damping in the liquid column of the TLCD. The statistical linearization method gives the following expression for the equivalent damping (assuming the liquid velocity to be Gaussian) as discussed in section 3.2.1:

$$c_f = \sqrt{\frac{2}{\pi}}\rho A \xi \sigma_{\dot{x}_f} \tag{5.1}$$

Equation 5.1 suggests that since $\sigma_{\dot{x}_f}$ increases as the loading increases, therefore, in order to maintain the optimal damping, ξ must decrease. Hence, there exists an optimal headloss coefficient at each loading intensity. These variations define the damping characteristics of the orifice needed at different excitation levels. An iterative method has been used in previous studies, (Balendra *et al*. 1995) since the damping term depends on $\sigma_{\dot{x}_f}$ which

is not known *a priori*. An alternative, which is a direct method is developed in this study. This involves evaluation of ζ_{opt} following the procedure outlined in the previous sections. This value is then substituted into Eq. 3.8 to obtain $\sigma_{\dot{x}_f}$. One can then determine ξ_{opt} using Eq. 5.1. Figure 5.2 provides a step by step flowchart for the two methods. Figure 5.3 (a) shows a typical iterative method for an SDOF-TLCD system subjected to white noise excitation, where σ_{X_s} and $\sigma_{\dot{x}_f}$ are calculated by Eqs. 3.8 and 3.9. This is repeated for a range of ξ, and ξ_{opt} is determined where the σ_{X_s} is minimum.

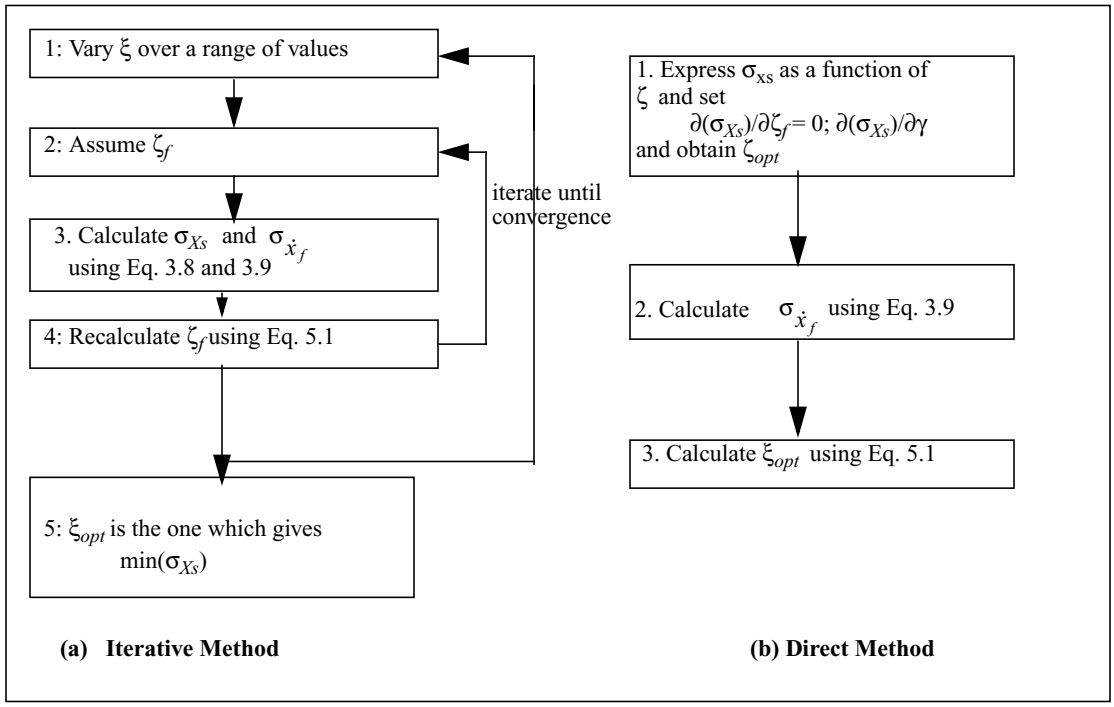

Figure 5.2 Flowchart of the two algorithms (a) iterative method (b) direct method

Explicit expressions to obtain ξ_{opt} for an undamped SDOF system subjected to white noise excitation with tuning ratio close to unity, can be obtained. The optimum value of the damping coefficient for this case reduces to the expression given in Eq. 3.12. After some manipulation, Eq. 3.12 and 5.1 provide,

$$\xi_{opt} = \mu\sqrt{\frac{(1+\mu-\alpha^2\mu)}{S_0}\left(\frac{\mu+\alpha^2}{1+\mu}\right)^{3/2} gl\omega_d\sqrt{\mu}} \tag{5.2}$$

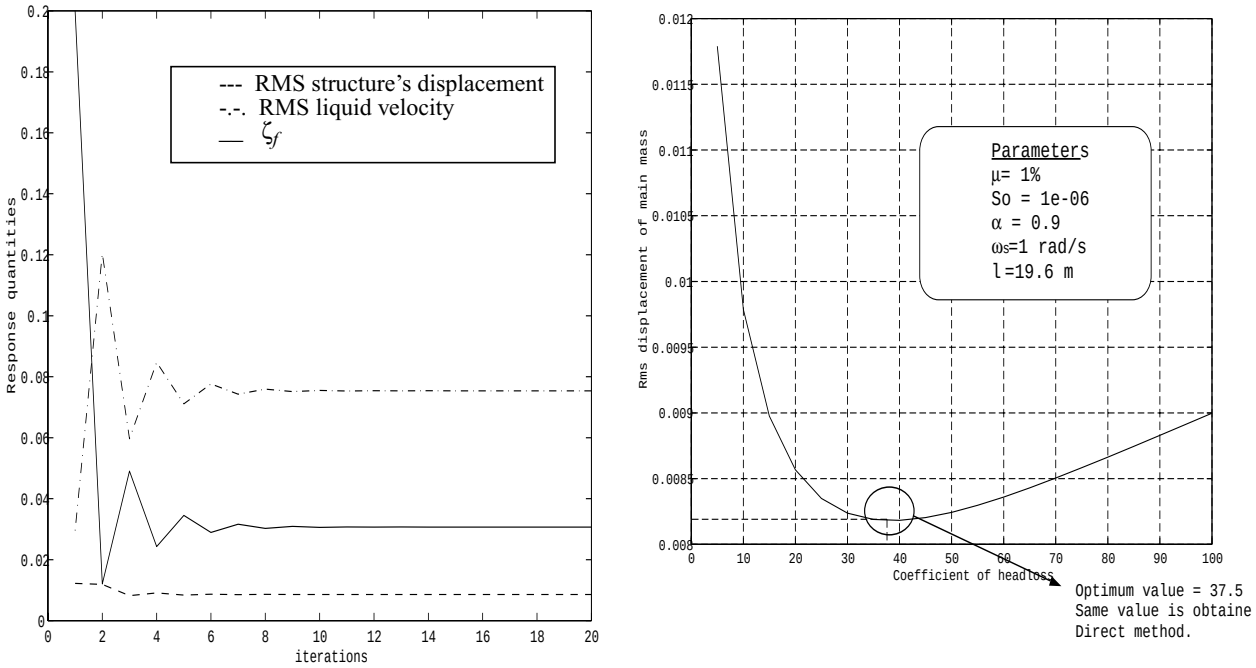

Figure 5.3 Iterative method (a) convergence of response quantities (b) optimum headloss coefficient

For tuning ratios not equal to unity, one can obtain similar expressions. However, they are cumbersome and can be obtained numerically. It is noteworthy from Eq. 5.2 that the optimum headloss coefficient is indirectly proportional to the square root of the intensity of white noise. Using some representative values, it can be shown that the direct (Eq. 5.2) and the iterative methods yield the same values (Fig. 5.3 (b)). However, the direct method is computationally superior, since it does not require iterations, making it more attractive for on-line semi-active control of the orifice.

Figure 5.4 shows the variation in the optimum headloss coefficient for various mass ratios of an SDOF-TLCD system under white noise excitation case. It is noted from these curves that at high loading intensities, very low headloss coefficients are needed. For

typical orifice characteristics, this corresponds to a hundred percent orifice opening ratio, i.e., the orifice should be fully open. At high amplitudes of excitation, it is, therefore, better to keep the orifice fully open and let the damping be provided by the liquid velocity. For low amplitudes of excitation, the liquid velocity is inadequate, therefore, the orifice opening should be decreased (thereby increasing ξ). The relationship between the orifice opening ratio and the headloss coefficient for standard orifices can be found in the literature (Blevins, 1984).

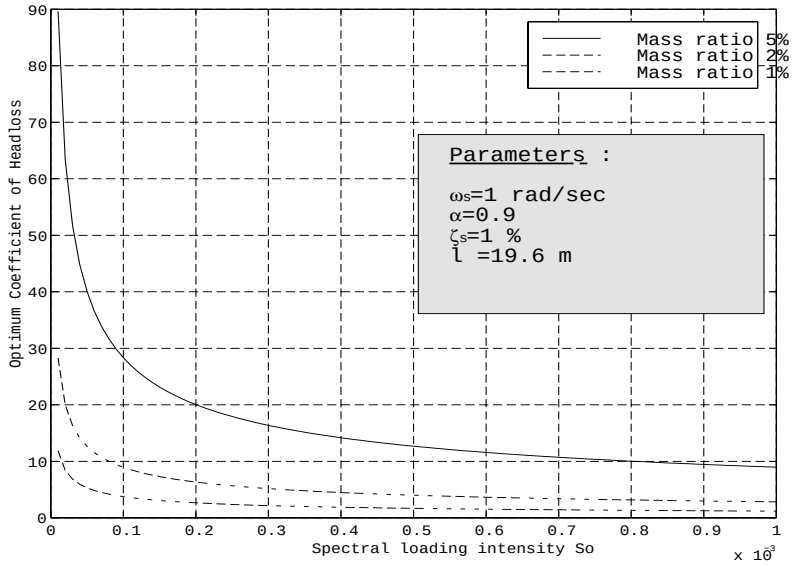

Figure 5.4 Variation of optimum headloss coefficient with loading intensity: white noise excitation

5.3 Applications

Two examples of semi-active system using *gain-scheduling* are presented in this section. The first example is for an SDOF-TLCD under random white noise excitation. The second example discusses the application of these dampers to an offshore structure.

5.3.1 Example 1: SDOF-TLCD system under random white noise

The efficiency of the *gain-scheduled* control can be seen from Fig. 5.5. The *look-up* table defined in Fig. 5.4 is used to introduce the semi-active control law. The parame-

ters of this system are as shown in Fig. 5.4. The efficiency of the passive TLCD is improved as the intensity of the white noise excitation changes from $So = 10^{-6}$ m^2/sec^3/Hz to $So = 10^{-4}$ m^2/sec^3/Hz (Table 5.1). Note that in the first segment of the loading, the performance of the semi-active and the passive system coincide with each other.

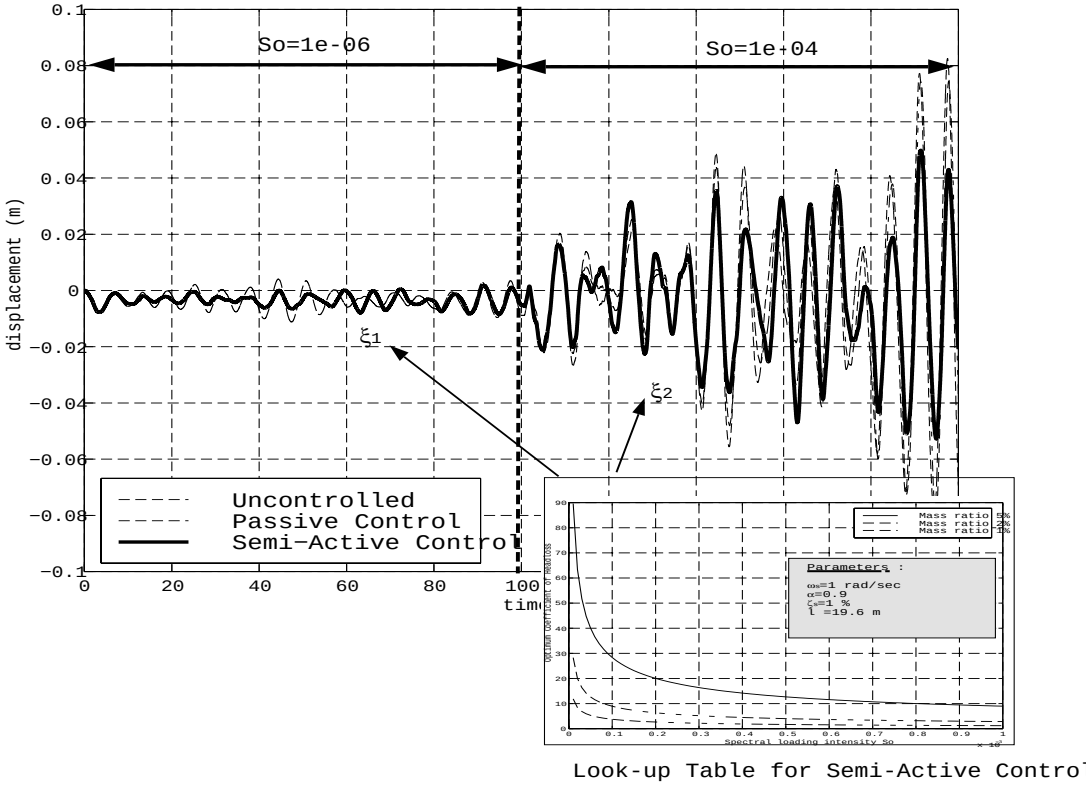

Figure 5.5 Example 1: SDOF system under random excitation.

TABLE 5.1 Comparison of different control strategies: Example 1

Control Case	*RMS Displacement of Primary system under random excitation* $So = 10^{-6}$ m^2/sec^3/Hz (m)	*RMS Displacement of Primary System under random excitation* $So = 10^{-4}$ m^2/sec^3/Hz (m)
Uncontrolled System	3.2 X 10^{-3}	2.77 X 10^{-2}
Passive System	2.1 X 10^{-3} (34.4%)	2.7 X 10^{-2} (2.5%)
Semi-active System	2.1 X 10^{-3} (34.4%)	2.09 X 10^{-2} (24.5%)

(Numbers in brackets indicate improvement of each control strategy over uncontrolled case)

5.3.2 Example 2: Application to Offshore Structure

The forces acting on most offshore structures are due to wind, waves and ocean currents. The motion of offshore structures is highly undesirable as it causes fatigue and shutdown of operations. In this section, a TLCD is proposed for control of offshore structures. The offshore structure has been idealized as a SDOF system as shown in Fig. 5.6(a). It is noteworthy that unlike land-based structures, platforms experiencing motions in ocean waves acquire additional mass and damping referred to as added mass and hydrodynamic damping. The mass, stiffness and damping can be written as (Brebbia *et al*. 1975):

$$M = l_c \rho_c A_c \int_0^1 [f(\bar{z})]^2 d\bar{z} + C_M l_c \int_0^1 [f(\bar{z})]^2 d\bar{z} + M_c \tag{5.3}$$

$$K = \frac{EI}{l_c^3} \int_0^1 \left(\frac{\partial^2}{\partial \bar{z}^2} f(\bar{z}) \right)^2 d\bar{z} \tag{5.4}$$

$$\omega_s = \sqrt{\frac{K}{M}} \tag{5.5}$$

$$C = C_s + C_D \sqrt{\frac{8}{\pi}} \int_0^1 \sigma_{\dot{Y}} [f(\bar{z})]^2 d\bar{z} \tag{5.6}$$

$$\sigma_{\dot{Y}}^2 = \int_0^\infty S_{\dot{Y}\dot{Y}}(\omega) d\omega = \int_0^\infty \omega^2 \left(\frac{\cosh kz}{\sinh kD} \right)^2 S_{\tilde{\eta}\tilde{\eta}}(\omega) d\omega \tag{5.7}$$

where $\bar{z} = \frac{z}{l_c}$, l_c is the length of the column, $k = \omega^2 / g$, g is the acceleration due to gravity, ω is the frequency, $f(\bar{z})$ is the assumed shape of the column, EI is the equivalent stiffness of the column, A_c is the equivalent area of the column, ρ is the density of water, M_c is the mass of the platform, C_D, C_M and C_A are the drag and inertia coefficients, and

$S_{\tilde{\eta}\tilde{\eta}}(\omega)$ is the spectra of wave elevation. The forcing function under the action of linear waves can be expressed as:

$$F(\omega, t) = \frac{\tilde{\eta}(C_M + C_A)\omega^2}{\sinh(kD)}\int_0^D \cosh(kz) f(\bar{z}) dz + \tilde{\eta} C_D \sqrt{\frac{8}{\pi}} \frac{\omega}{\sinh(kD)} \int_0^D \cosh(kz) \sigma_{\dot{V}} f(\bar{z}) dz \tag{5.8}$$

The shape of the deflected platform is approximated as $f(\bar{z}) = \bar{z}^2$ and hence the mass of the system is calculated using Eq. 5.3 as M = 7.72 X 10^6 Kg and stiffness, K = 9 X 10^6 N/m using Eq. 5.4. This results in a natural frequency of the structure, ω_s = 1.07 rad/s. The total damping ratio of the structure is evaluated using Eq. 5.6 which is equal to 6%. The drag and inertia coefficients for the equivalent column are: $C_D = c_d \rho D/2$ = 5000 Kg/m^2; $C_M = c_m \rho V_W$ = 78000 Kg/m and $C_A = \rho V_W$ = 78000 Kg/m (with c_m=c_d=1).

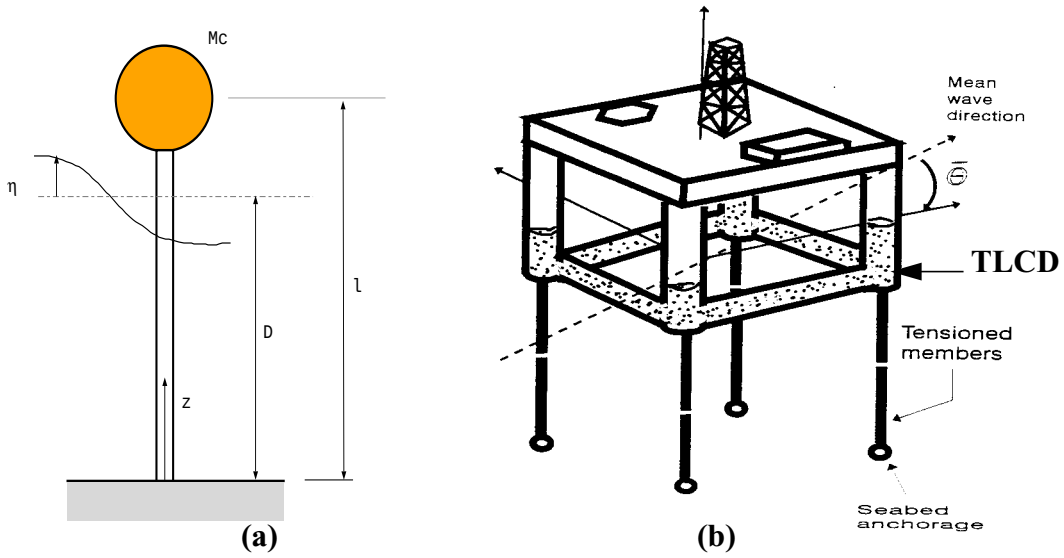

Figure 5.6 (a) Single degree of freedom idealization of an offshore structure (b) Concept of Liquid Dampers in TLPs

TABLE 5.2 Numerical parameters used: Example 2

Parameter	Numerical Value	Parameter	Numerical Value
Depth of water, D	75 m	EI value	2250 X10^9 Nm^2
Mass of Platform, M_c	2 X10^6 Kg	Density of water, ρ	1000 Kg/m^3
Length of Structure, l_c	100 m	length of liquid damper, l	18 m
Cross sectional Area, A_c	28 m^2	Area of damper (with μ=2%), A	8.8 m^2
Total Volume of water displaced per unit length, V_W	78 m^3/m	Density of Concrete, ρ_c	2500 Kg/m^3

The wave spectrum used in this study is the *Pierson and Moskowitz* (P-M) spectrum,

$$S_{\tilde{\eta}\tilde{\eta}}(\omega) = \frac{\alpha_1 g^2}{\omega^5}\exp\left(-\beta_1\left(\frac{g}{\omega U}\right)^4\right) \tag{5.9}$$

where U is the wind speed at 10 meters above the sea surface and α_1 , β_1 are dimensionless parameters which determine the shape of the spectrum. For the North Sea, the value of $\alpha_1 = 0.0081$ and $\beta_1 = 0.74$. In the frequency domain, the expression for the forcing function can be derived from Eq. 5.8, which can be written as,

$$S_{FF}(\omega) = S_{\tilde{\eta}\tilde{\eta}}(\omega)\left\{\frac{(C_M + C_A)^2\omega^4}{\sinh(kD)^2}\left(\int_0^D \cosh(kz) f(\bar{z}) dz\right)^2 + \frac{8C_D^2\omega^2}{\pi\sinh(kD)^2}\left(\int_0^D \cosh(kz)\sigma_{\dot{V}} f(\bar{z}) dz\right)^2\right\} \tag{5.10}$$

Figure 5.6 (b) shows a schematic of the possible design of liquid dampers functioning as pontoon water tanks of the Tension Leg platform (TLP). The wave forcing function on such platforms may not be ideally described by Eq. 5.8. This is because the size of the platform in comparison with the wave length of approaching waves is large, which results in diffraction of waves. Therefore, in this case the first component of the forcing function is obtained from diffraction analysis (Kareem and Li, 1988).

Optimal parameters are obtained using numerical optimization, as done previously in chapter 3, with the objective of minimizing the accelerations (*absorber efficiency* = ratio of RMS structural accelerations with and without the damper). As shown from Fig. 5.7, there exists optimum damper parameters, which are found to be independent of the loading conditions (i.e., different U_{10}). Therefore, under all loading conditions, these parameters must be maintained at their optimal values, otherwise the performance of the damper may deteriorate.

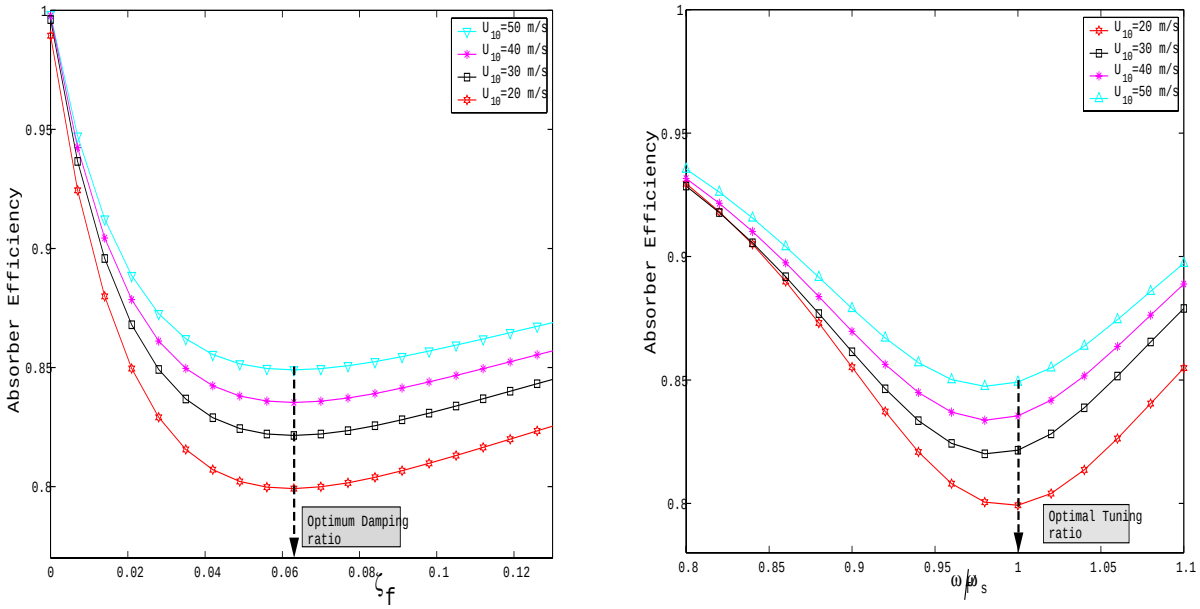

Figure 5.7 Optimal Absorber parameters as a function of loading conditions

Next, one can easily apply the *gain-scheduled* law described in the previous sections for semi-active control. The *look-up* table can be generated as shown in Fig. 5.8 (a) for different loading conditions. Figure 5.8(b) shows the spectra of structural acceleration as the headloss coefficient is changed. The mass ratio of the damper mass to the main mass is 2%. The space is very limited on a typical offshore structure and therefore, the pontoon tanks filled up with water can also be utilized as water supply for occupants. However, this

may not be always possible as water is used to ballast a platform and is restricted from sloshing to eliminate unnecessary sloshing forces on the hull.

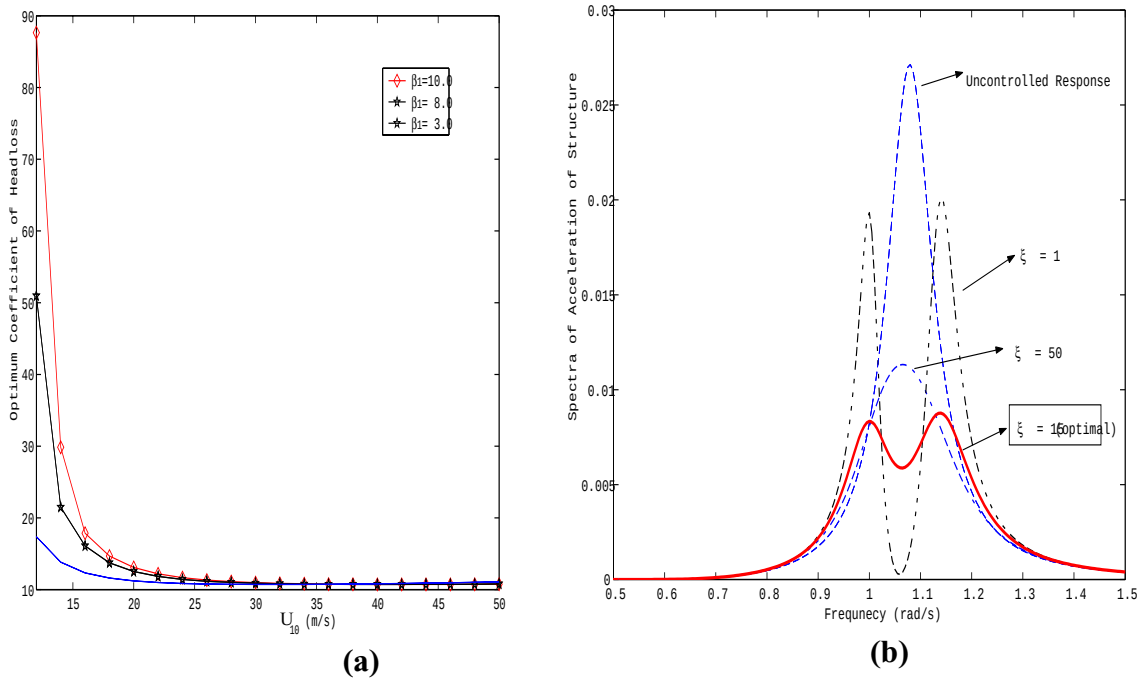

Figure 5.8 (a) Variation of Optimal Headloss Coefficient with loading conditions for different wave spectra (b) Spectra of structural acceleration at U_{10}=20 m/s for different ξ.

5.4 Clipped-Optimal System

The semi-active system described in this section requires a controllable orifice with negligible valve dynamics whose coefficient of headloss can be changed rapidly by applying a command voltage (Fig.5.9). This type of semi-active control is more suitable for excitations which are transient in nature, for e.g., sudden wind gusts or earthquakes. Equation 3.3 can be posed in an active control framework as follows:

$$\begin{bmatrix} \mathbf{M_s} + m_f & \alpha m_f \\ \alpha m_f & m_f \end{bmatrix} \begin{bmatrix} \ddot{\mathbf{X}}_s \\ \ddot{x}_f \end{bmatrix} + \begin{bmatrix} \mathbf{C}_s & 0 \\ 0 & 0 \end{bmatrix} \begin{bmatrix} \dot{\mathbf{X}}_s \\ \dot{x}_f \end{bmatrix} + \begin{bmatrix} \mathbf{K}_s & 0 \\ 0 & k_f \end{bmatrix} \begin{bmatrix} \mathbf{X}_s \\ x_f \end{bmatrix} = \begin{bmatrix} \mathbf{F}_e(t) \\ 0 \end{bmatrix} + \begin{bmatrix} 0 \\ 1 \end{bmatrix} u(t) \qquad (5.11)$$

where the bold face denotes matrix notation and *u(t)* is the control force given by:

$$u(t) = \frac{-\rho A \xi(t) |\dot{x}_f|}{2} \dot{x}_f \tag{5.12}$$

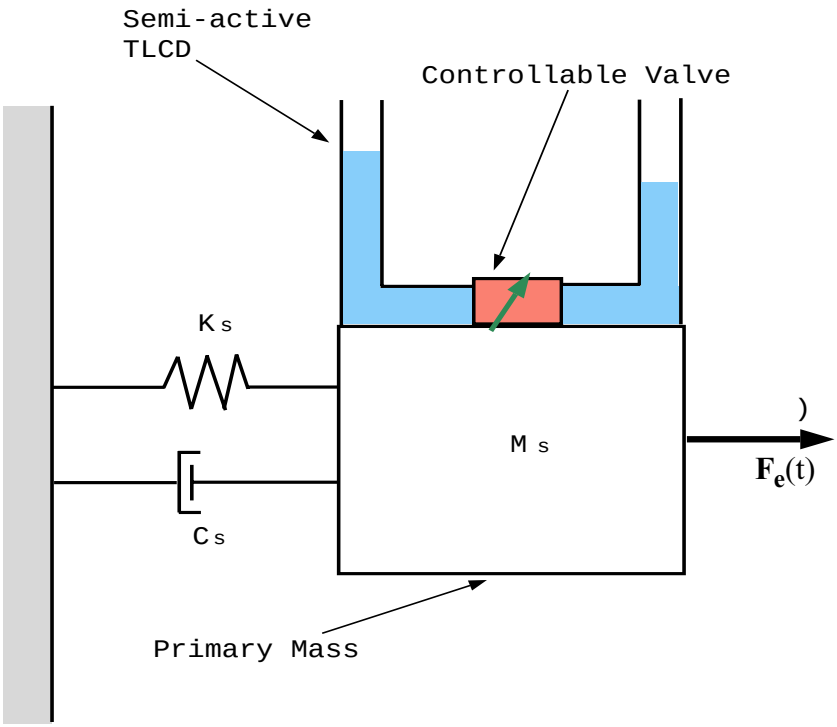

Figure 5.9 Semi-active TLCD-Structure combined system

The coefficient of headloss is an important parameter which is controlled by varying the orifice area of the valve. In the case of a passive system, this headloss coefficient is unchanged. The headloss through a valve/orifice is defined as:

$$h_l = \frac{\xi V^2}{2g} \tag{5.13}$$

where V is the velocity of the liquid in the tube. The coefficients of headloss for different valve openings are well documented for different types of valves (Lyons, 1982). The relationship between the headloss coefficient (ξ) and the valve conductance (C_V) is derived in Appendix A.3.

The damping force of a semi-active TLCD can be written as:

$$F_d(t) = \frac{\rho A \xi(\Lambda, t)}{2} |\dot{x}_f(t)| \dot{x}_f(t) \tag{5.14}$$

where $\xi(\Lambda, t)$ is the headloss coefficient, which is a function of the applied voltage Λ, needed to control valve opening, at a given time *t.* Equation 5.14 can be re-written as,

$$F_d(t) = \tilde{C}(\Lambda, t)|V|V \tag{5.15}$$

where $\tilde{C}(\Lambda, t) = \frac{\rho A \xi(\Lambda, t)}{2}$ and $V = \dot{x}_f(t)$. In this format, this damper system can be compared to typical variable damping fluid dampers. Semi-active fluid viscous dampers have been studied among others by Symans *et al*. 1997 and Patten *et al.* (1998). The damping force in such a system can be written as:

$$F_d(t) = C(\Lambda, t)\underset{\sim}{V} \tag{5.16}$$

where $C(\Lambda)$ is the damping coefficient which is a function of the command voltage Λ and $\underset{\sim}{V}$ is the velocity of the piston head. The damping coefficient is bounded by a maximum and a minimum value and may take any value between these bounds.

Comparing Eqs. 5.15 and 5.16, one can some similarity in the fundamental working of these dampers. However, there are basic differences in the two physical systems. In variable orifice dampers, the fluid is viscous, usually some silicone-based material, which is orificed by a piston. In the TLCD case, the liquid is usually water and is under atmospheric pressure. Moreover, the damping introduced by an orifice in a TLCD system is quadratic in nature, whereas the damping imparted by a fluid damper is linear (Kareem and Gurley, 1996).

5.4.1 Control Strategies

Most semi-active strategies are inherently non-linear due to the non-linearities introduced by the device in use. Therefore, a great deal of research is based on developing innovative algorithms for implementing semi-active strategies. Some of the common examples are sliding mode control and nonlinear H_∞ strategies (Yoshida *et al.* 1998). Some innovative algorithms involving shaping of the force-deformation loop in a variable damper system are reported in Kurino and Kobori, 1998. Other researchers have used fuzzy control theories to effectively implement semi-active control (e.g., Sun and Goto, 1994; Symans and Kelly, 1999).

The strategy considered in this study is based on the linear optimal control theory. The negative sign in Eq. 5.12 ensures that the control force is always acting in a direction opposite to the liquid velocity. In case, the liquid velocity and the desired control force are of the same sign, then Eq. 5.12, implies that ξ is negative. Since it is not practical to have a negative coefficient of headloss, the control strategy sets it to a minimum for ξ, i.e., ξ_{min}. The control force is regulated by varying the coefficient of headloss in accordance with the semi-active control strategy given as follows:

$$\xi(t) = -2u(t)/(\rho A|\dot{x}_f|\dot{x}_f) \le \xi_{max} \qquad \text{if } (u(t)\dot{x}_f(t)) < 0$$

$$\xi(t) = \xi_{min} \qquad \text{if } (u(t)\dot{x}_f(t)) \ge 0 \tag{5.17}$$

In a fully active control system, one needs an actuator to supply the desired control force. In such a case, the control force is not constrained to be in a direction opposite to the damper velocity. Therefore, the linear control theory is readily applicable to active control systems. In case of semi-active systems, however, the proposed control law is a *clipped*

optimal control law since it emulates a fully active system only when the desired control force is dissipative (Karnopp *et al.* 1974; Dyke *et al.* 1996). Moreover, the actual control force that can be introduced is dependent on the physical limitations of the valve used and the maximum coefficient of the headloss it can supply, which implies bounds on the control force introduced. This bound is given by,

$$\left(\frac{-\rho A \xi_{min} |\dot{x}_f|}{2} \dot{x}_f\right) \leq u(t) \leq \left(\frac{-\rho A \xi_{max} |\dot{x}_f|}{2} \dot{x}_f\right) \tag{5.18}$$

A slight variation of the preceding *continuously-varying* orifice control is the commonly used *on-off* control. Most valve manufactures supply valves which operate in a bi-state: fully open or fully closed. These valves require a two-stage solenoid valve. On the other hand, the *continuously-varying* control requires a variable damper which utilizes a servovalve. This servovalve is driven by a high response motor and contains a spool position feedback system, and therefore is more expensive and difficult to control than a solenoid valve. The *on-off* control is simply stated as:

$$\xi(t) = \xi_{max} \qquad \text{if } (u(t)\dot{x}_f(t)) < 0$$

$$\xi(t) = \xi_{min} \qquad \text{if } (u(t)\dot{x}_f(t)) \geq 0 \tag{5.19}$$

ξ_{min} can be taken as zero because this corresponds to the fully opened valve. It can be expected that a small value of ξ_{max} will result in a lower level of response reduction.

In order to formulate the system in a state space format, Eq. 5.11 is recast as,

$$\mathbf{M}\ddot{\mathbf{x}}(t) + \mathbf{C}\dot{\mathbf{x}}(t) + \mathbf{K}\mathbf{x}(t) = \mathbf{E_1}\mathbf{W}(t) + \mathbf{B_1}u(t) \tag{5.20}$$

which is then expressed in the state-space form,

$$\dot{\mathbf{X}} = \mathbf{A}\mathbf{X} + \mathbf{B}u + \mathbf{E}\mathbf{W} \tag{5.21}$$

where $\mathbf{X} = \begin{bmatrix} \mathbf{x} \\ \dot{\mathbf{x}} \end{bmatrix}$; $\mathbf{A} = \begin{bmatrix} \mathbf{0} & \mathbf{I} \\ -\mathbf{M}^{-1}\mathbf{K} & -\mathbf{M}^{-1}\mathbf{C} \end{bmatrix}$; $\mathbf{B} = \begin{bmatrix} \mathbf{0} \\ \mathbf{M}^{-1}\mathbf{B_1} \end{bmatrix}$; and $\mathbf{E} = \begin{bmatrix} \mathbf{0} \\ \mathbf{M}^{-1}\mathbf{E_1} \end{bmatrix}$ and

$\mathbf{E_1}$ and $\mathbf{B_1}$ are the control effect and loading effect matrices, respectively. The states of the system are the displacements and velocities of each lumped mass of the structure and the displacement and velocity of the liquid in the TLCD. Measurements of the structural response can be expressed as:

$$\mathbf{Y} = \mathbf{C}\mathbf{X} + \mathbf{D}u + \mathbf{F}\mathbf{W} \tag{5.22}$$

where $\mathbf{C} = [\mathbf{I}]$; $\mathbf{D} = [\mathbf{0}]$; and $\mathbf{F} = [\mathbf{0}]$ in the case of full state feedback. The desired optimal control force is generated by solving the standard Linear Quadratic Regulator (LQR) problem. The main idea in LQR problem is to formulate a feedback control law which would minimize the cost function given as $J = \lim_{T \to \infty} E\left\{\int_0^T (\boldsymbol{Z}^T \boldsymbol{Q} \boldsymbol{Z} + u^T R u)dt\right\}$,

where **Q** and R are the control matrices for the LQR strategy. The control force is obtained by,

$$u = -\mathbf{K}_g\mathbf{X} \tag{5.23}$$

where $\boldsymbol{K}_g$ is the control gain vector and is given as:

$$\mathbf{K}_g = \mathbf{R}^{-1}\mathbf{B}^T\mathbf{P} \tag{5.24}$$

and **P** is the *Riccati* matrix obtained by solving the matrix *Riccati* equation:

$$\mathbf{P}\mathbf{A} - \mathbf{P}\mathbf{B}(\mathbf{R}^{-1}\mathbf{B}^T\mathbf{P}) + \mathbf{A}^T\mathbf{P} + \mathbf{Q} = \mathbf{0} \tag{5.25}$$

A schematic diagram of the control system is depicted in Fig. 5.10.

The control performance of each strategy is evaluated based on a prescribed criterion. For this purpose appropriate performance indices, regarding the RMS displacements $\langle X_s \rangle$, accelerations of the structure $\langle \ddot{X}_s \rangle$, and the effective control force $\langle u \rangle$ are defined below:

$$J_1 = \frac{(\langle X_s \rangle_{unco} - \langle X_s \rangle_{co})}{\langle X_s \rangle_{unco}} \; ; \; J_3 = \frac{(\langle \ddot{X}_s \rangle_{unco} - \langle \ddot{X}_s \rangle_{co})}{\langle \ddot{X}_s \rangle_{unco}} \; ; \; J_u = \langle u \rangle \qquad (5.26)$$

where subscripts *unco* and *co* are used to distinguish between uncontrolled and controlled cases.

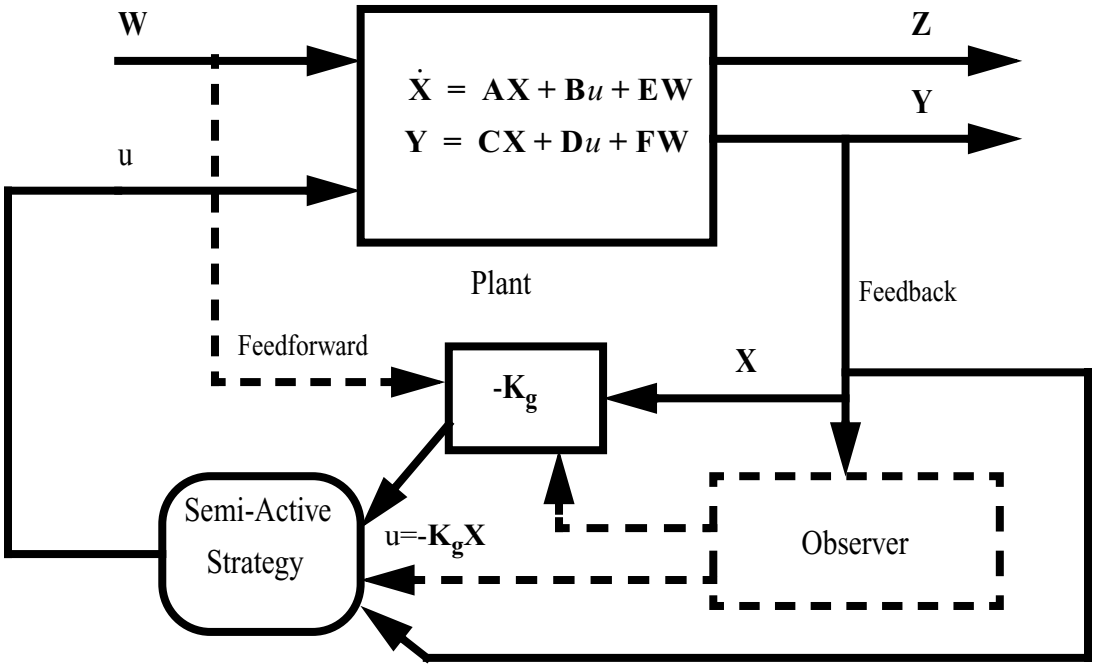

Figure 5.10 Schematic of the control system

In actual practice, it is more realistic to consider a few noisy measurements which are then used to estimate the system states. In this situation, the standard stochastic Linear Quadratic Gaussian (LQG) framework is used for estimation (Maciejowski, 1989). In a stochastic framework, the measurements are given as,

$$\mathbf{Y} = \mathbf{C}\mathbf{X} + \mathbf{D}u + \mathbf{F}\mathbf{W} + \tilde{\nu} \tag{5.27}$$

where $\tilde{\nu}$ is the measurement (sensor) noise which is invariably present in all measurements. The LQG problem is solved using the *seperation principle* which states that first an optimal estimate $\hat{\boldsymbol{X}}$ of the states $\boldsymbol{X}$ (optimal in the sense that $E\{(\boldsymbol{X} - \hat{\boldsymbol{X}})^T(\boldsymbol{X} - \hat{\boldsymbol{X}})\}$ is minimized) is obtained, and then this is used as if it were an exact measurement to solve the determinstic LQR problem discussed earlier. From the measurements, the states of the system $\hat{\mathbf{X}}$ can be estimated using a *Luenberger* observer:

$$\dot{\hat{\mathbf{X}}} = \mathbf{A}\hat{\mathbf{X}} + \mathbf{B}u + \mathbf{L}(\mathbf{Y} - \mathbf{C}\hat{\mathbf{X}} - \mathbf{D}u) \tag{5.28}$$

where $\mathbf{L}$ is determined using standard *Kalman-Bucy* filter estimator techniques. The optimal control is then written as:

$$u = -\mathbf{K}_g\hat{\mathbf{X}} \tag{5.29}$$

where $\mathbf{K_g}$ is the optimal control gain matrix obtained by solving the standard LQR problem as discussed previously.

5.4.2 Example 3: MDOF system under random wind loading

The first example is an MDOF-TLCD system, as shown in Fig. 5.11, which is a high rise building subjected to alongwind aerodynamic loading. The building dimensions are 31 m X 31 m in plan and 183 m tall. The structural system is lumped at five levels and natural frequencies of this building are: 0.2, 0.583, 0.921, 1.182, and 1.348 Hz. The corresponding modal damping ratios are 1%, 1.57%, 2.14%, 2.52% and 2.9%. The description of the wind loading and the structural system matrices for mass, stiffness and damping are given in Li and Kareem (1990).

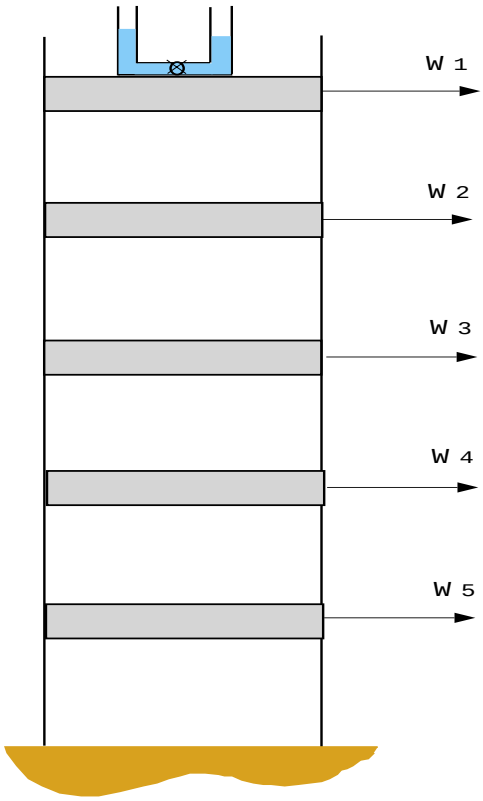

Figure 5.11 Schematic of 5DOF building with semi-active TLCD on top story

The TLCD is designed such that the ratio of the mass of liquid in TLCD to the first generalized mass of the building was 1%, the length ratio, $\alpha = 0.9$ and ξ_{max}=15. Using a multi-variate simulation approach (Li and Kareem, 1993), wind loads were simulated at the five levels, as shown in Fig. 5.12. Two types of semi-active strategies, namely the c*on-tinuously-varying* and the *on-off* type were examined. The LQR method, as described in the earlier section, was used to determine the control gains. It was assumed that all states were available to provide the feedback.

The results are summarized in Fig. 5.13 and Table 5.3. As seen from Table 5.3, the semi-active strategies provide an additional 10-15% reduction over passive systems. Table 5.3 also shows how the two semi-active strategies deviate from the optimal control force.

One can observe the sub-optimal performance of these schemes, which leads to a lower response reduction than the active case. In a semi-active system, the applied control force is generated using a controllable valve which can be operated using a small energy source such as a battery.

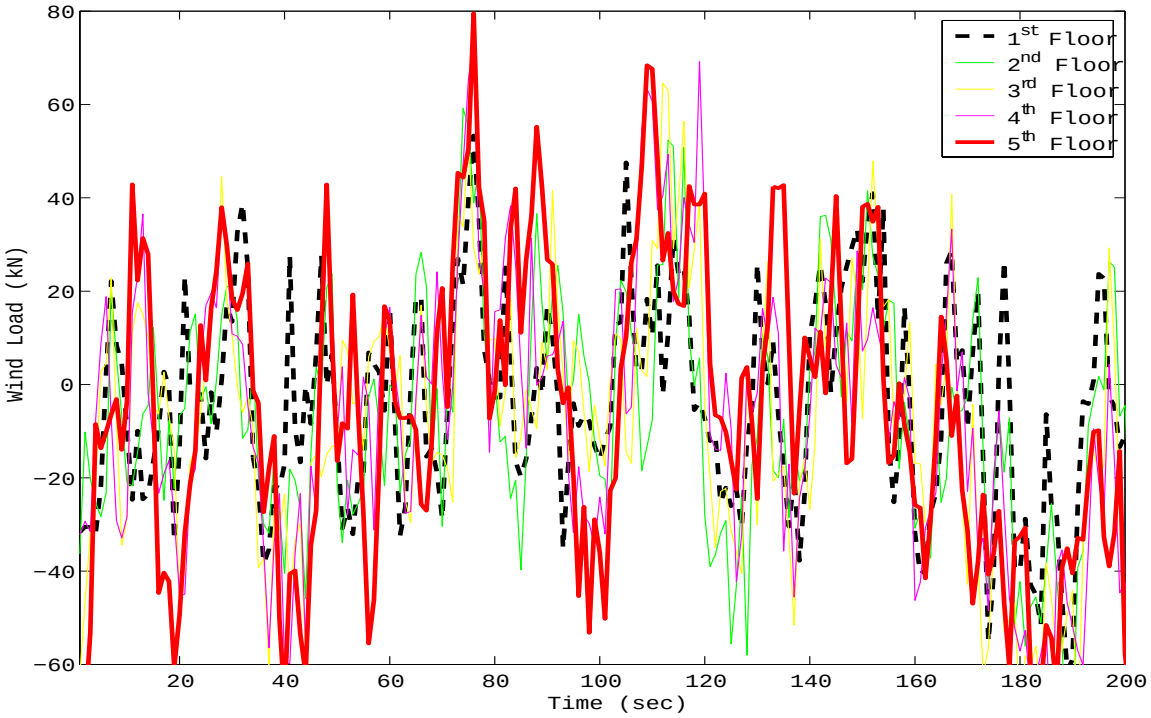

Figure 5.12 Wind loads acting on each lumped mass

TABLE 5.3 Comparison of various control strategies: Example 3

Control Case	RMS Disp. (cm) and (J_1) (%)	RMS accel. (cm/s^2) and (J_3) (%)	RMS control force (kN) Ju
Uncontrolled	7.05	10.61	-
Passive TLCD	5.24 (25.6%)	7.63 (28.0%)	-
Continuously varying	4.84 (31.2%)	6.84(35.3%)	79.8 (Eq. 5.12, 5.17)
On-Off control	4.83 (31.2%)	6.84 (35.3%)	79.9 (Eq. 5.12, 5.19)
Active control	2.51 (64.4%)	4.87 (55.0%)	133.8 (Eq. 5.23)

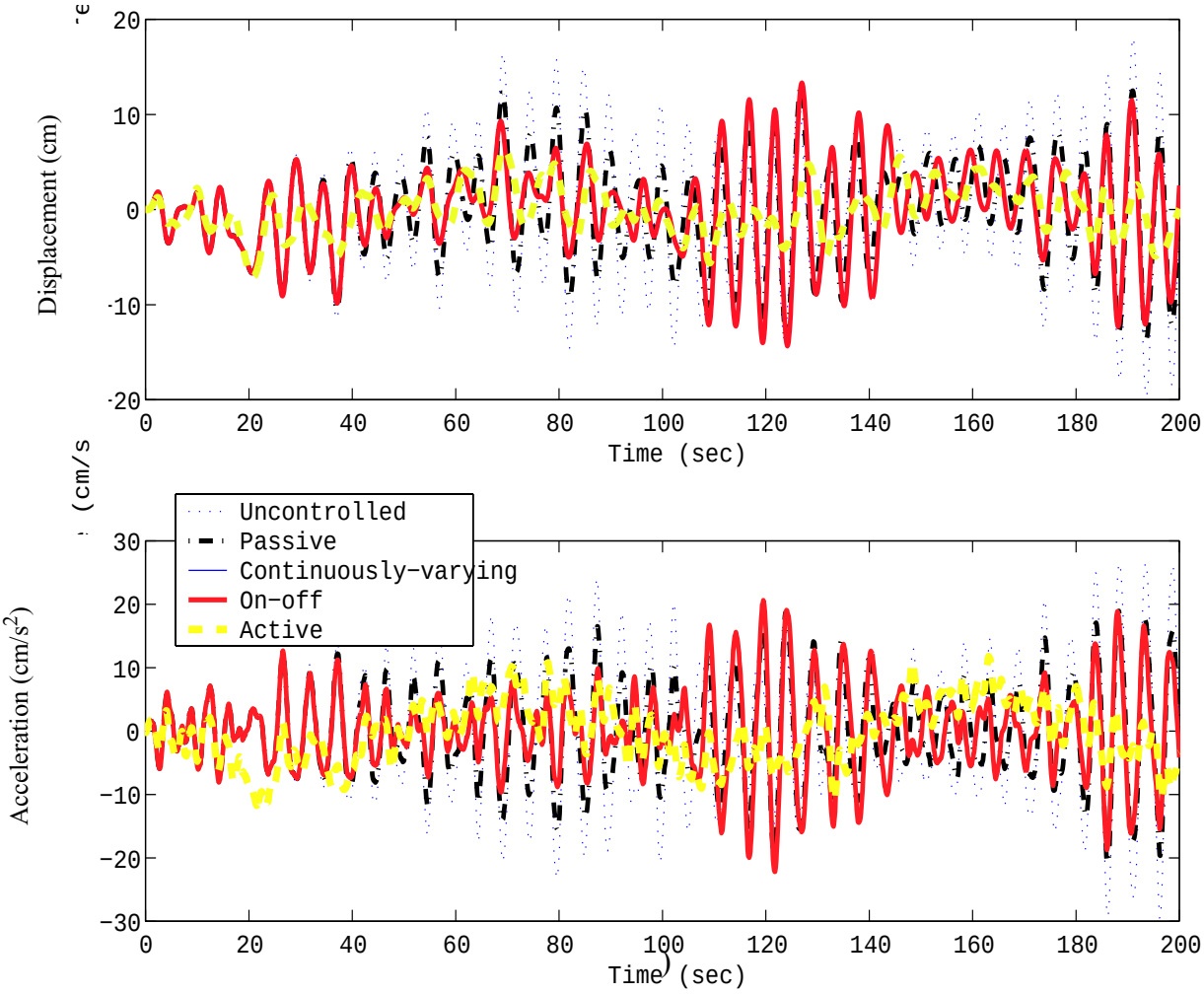

Figure 5.13 Displacements and Acceleration of Top Level using various control strategies

5.4.3 Example 4: MDOF system under harmonic loading

In the next example, a multi degree of freedom (5DOF) system is considered again, but under harmonic loading. This example is taken from Soong (1991). The lumped mass on each floor is 131338.6 tons and the damping ratio is assumed to be 3% in each mode. The natural frequencies are computed to be 0.23, 0.35, 0.42, 0.49 and 0.56 Hz. A vector of harmonic excitation is defined:

$$\mathbf{W}(t) = \mathbf{a}\cos(\omega t) + \mathbf{b}\cos(2\omega t) + \mathbf{c}\cos(3\omega t) + \mathbf{d}\sin(4\omega t) \qquad (5.30)$$

where ω = 1.47 rad/s (= first natural frequency of the structure), and the values of **a**, **b**, **c** and **d** and the stiffness matrix of the structure are given in Appendix A.2. The excitation acts at a frequency equal to the first natural frequency of the structure. The semi-active TLCD is placed on the top floor of the building with similar parameters as in Example 3. Two cases of control strategies are considered: (a) full state feedback, and (b) acceleration feedback using observer based controllers.

Full state-feedback LQR strategy

The first strategy assumes that all states are available for feed-back (total of 12 measurements). The control gains are calculated using Eq. 5.24. Figure 5.14 shows the parametric variation of J_1, J_2 and J_u as a function of $\xi_{max.}$ There are small reductions in the response after a certain value of ξ_{max} is reached. This can be explained by Eq. 5.18 in which it is implied that the applied control force is constrained by ξ_{max}. This means that satisfactory control results can be achieved by choosing a valve which may have a limited range of headloss coefficients.

Figure 5.15 shows the response of the top floor of the structure using various control strategies. It is noteworthy that the *continuously varying* and *on-off* strategies give similar reduction in response. This can be explained by the results in Fig. 5.16. The profiles of variation in the headloss coefficient as a function of time are similar for the two strategies. The *continuously varying* control gives flexibility in the headloss coefficient. However, the saturation bound introduces a clipping effect similar to *on-off* control and therefore in this case, the advantage of *continuously-varying* control strategy is lost. Figure 5.17 shows the RMS displacement of the floor displacements and accelerations, maximum story shear and maximum inter-story displacements using various control strategies.

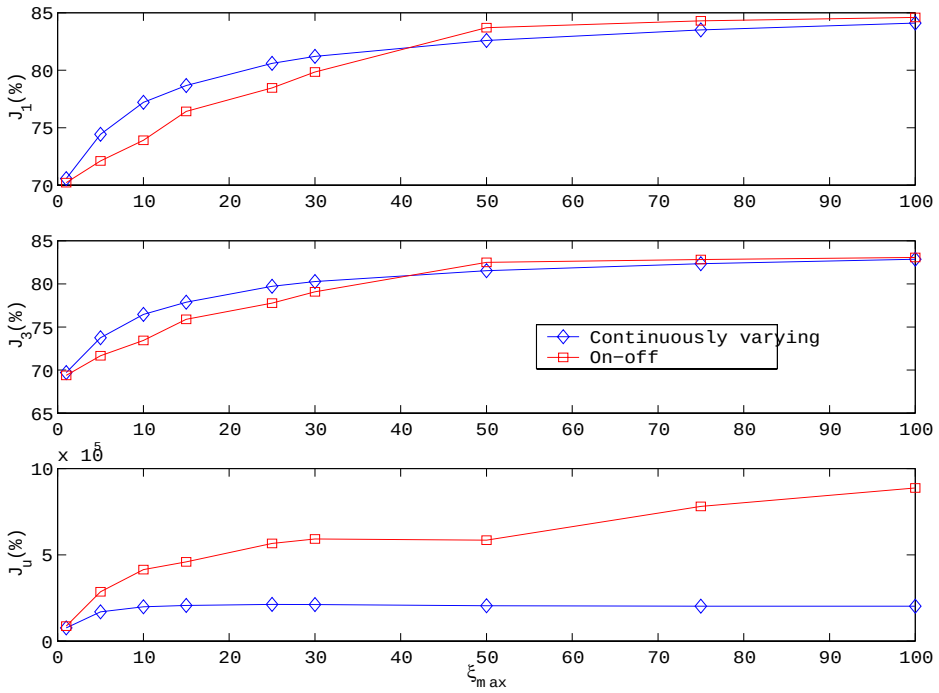

Figure 5.14 Variation of performance indices with maximum headloss coefficient

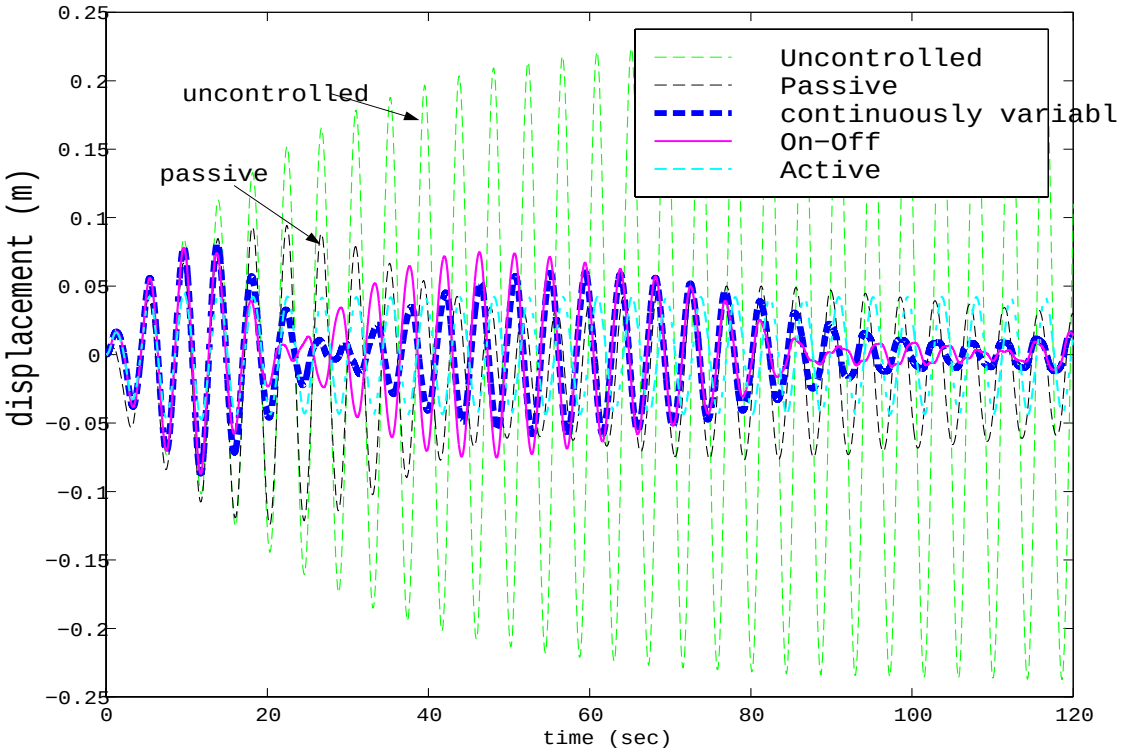

Figure 5.15 Displacement of Top Floor under various control strategies

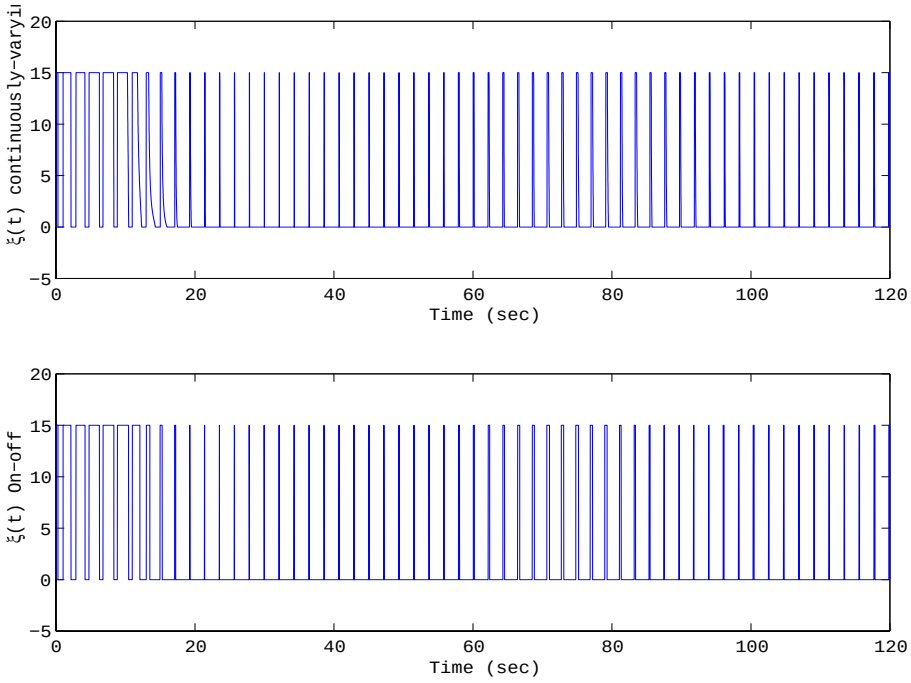

Figure 5.16 Variation of headloss coefficient with time

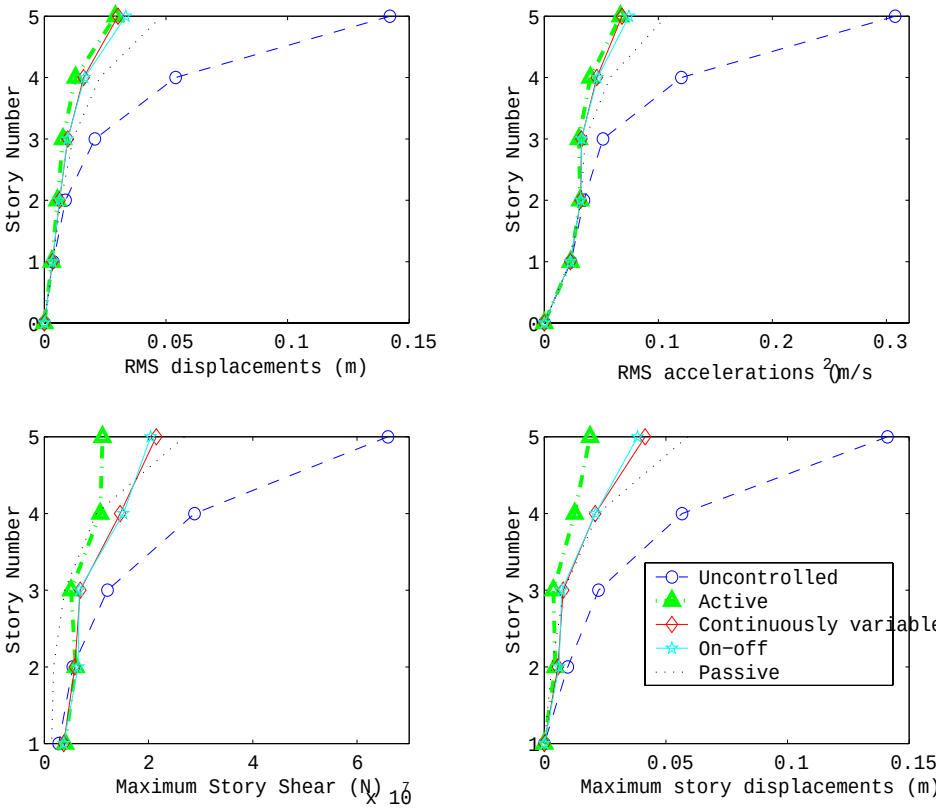

Figure 5.17 Variation of RMS displacements, RMS accelerations, maximum story shear and maximum inter-story displacements

Observer-based LQG strategy

In the previous case, it was conveniently assumed that all the states were available for feedback. However, in practice only a limited number of measurements are feasible. In this case, we assumed that the floor accelerations and the liquid level (displacement of the liquid) were measured. This implied that there were a total of six measurements (five accelerations and one liquid displacement). The measurement noise was modeled as Gaussian rectangular pulse processes with a pulse width of 0.002 seconds and a spectral intensity of 10^{-9} m^2 /sec^3/Hz. A comparison of the various strategies using observer-based LQG control is presented in Table 5.4. The response reduction is similar to the results obtained using LQR control.

TABLE 5.4 Comparison of various control strategies: Example 4

Control Case	RMS Displacement (cm)/ (J_1 %)	RMS acceleration (cm/s^2)/ (J_3 %)	RMS control force (kN) Ju	No. of measure-ments
Uncontrolled	14.21	30.78	-	-
Passive TLCD	4.82 (66.08)	10.72 (65.17)	-	-
Active case	2.92 (79.45)	6.67 (78.33)	188 (Eq. 5.23)	12
Continuously varying	3.03 (78.68)	6.81 (77.88)	171.6 (Eq. 5.12, 5.17)	12
On-Off control	3.35 (76.43)	7.43 (75.86)	203.1(Eq. 5.12, 5.19)	12
Continuously Varying OBSERVER BASED	3.21 (77.41)	7.58 (75.37)	70.4 (Eq. 5.12, 5.17)	6
On-Off control OBSERVER BASED	3.13 (77.97)	8.43 (72.61)	170.7 (Eq. 5.12, 5.19)	6

5.5 Concluding Remarks

Two types of semi-active systems were presented in this chapter. The first was based on a *gain-scheduled* feedforward type of control which utilized a *look-up* table for control action. The second was a *clipped-optimal* feedback control system with *continuously-varying* and *on-off* type of control.

Numerical examples and applications were presented for the *gain-scheduled* control. This type of semi-active system leads to 15-25% improvement over a passive system. An application of these systems for offshore structures was also presented.

Next, the *clipped-optimal* control was discussed. The efficiency of the state-feedback and observer-based control strategy was compared. Numerical examples showed that semi-active strategies provide better response reduction than the passive system for both random and harmonic excitations. In the case of harmonic loading, the improvement was about 25-30% while for the random excitation, the improvement was about 10-15%. It was also noted that *continuously-varying* semi-active control algorithm did not provide a substantial improvement in response reduction over the relatively simple *on-off* control algorithm.